Supporting Information

Modulating M-S Motifs of the Metallic Electrocatalyst with Low Overpotential for Hydrogen Evolution Reaction in Acidic Electrolyte

Nannan Zhao[a†*], Fei Lin[c†], Guobin Wen[a*], Na Tang[b], Penggao Cheng[b], Lei Zhang[b], and Lifeng Liu[c*]

[a] N. Zhao and G. Wen
College of Chemistry and Chemical Engineering
Hunan University
Changsha, Hunan 410082, China.
E-mail: zhaonannan2023@hnu.edu.cn, gbwen@hnu.edu.cn
[b] N. Tang, P. Cheng and L. Zhang
Tianjin Key Laboratory of Brine Chemical Engineering and Resource Eco-utilization,
Tianjin University of Science & Technology, Tianjin 300457, China.
[c] F Lin and L Liu
Songshan Lake Materials Laboratory (SLAB), Dongguan 523808, P. R. China.
E-mail: liu.lifeng@sslab.org.cn
Nannan Zhao and Fei Lin contributed equally to this work.
*Corresponding author (Dr, N Zhao, Prof. Dr, G. Wen and Prof. Dr, Lifeng Liu).

Table of contents

Methods

1.1 Materials

Carbon cloth (CC, 0.32 mm thickness, Electronic Materials Management Department), Nitric acid (HNO_3, 36.0%-38.0%, Tianjin Jiangtian Chemical Technology Co., Ltd.), Sulfur powder (S, 99.5%, Aladdin), Ruthenium oxide (RuO_2, 99%, Shanghai Aladdin Biochemical Technology Company), Platinum (Pt/C, nominally 20% on carbon black, Alfa Aesar) and Nafion solution (5%, DuPont) were used without further purification. Sodium chloride (NaCl, ≥99.5%), sulfuric acid (H_2SO_4, reagent grade) was purchased from Aldrich Chemical. All chemicals and reagents were used without any further purification.

1.2 Synthesis of catalysts

Initially, a piece of carbon cloth (CC, 1.0 cm × 2.0 cm) was treated in 3.0 m HNO_3 solution for 5 hours at 60 °C and cleaned several times with ethanol and ultrapure water.

Then, FeNiCoS were directly grown on the carbon cloth with various ratio of Ni, Co and Fe compound. FeNiCoS was first synthesized using the synthesized by a solvothermal method by controlling organic precursors growth. Mixing of the solution and carbon cloth was then transferred to Teflon-lined stainless-steel autoclave and maintained at 120 °C for 6 hours and then dried at 60 °C overnight. Then, the precursors were pyrolyzed in air for 2 h to gain FeNiCoO.

Next, the simple high-temperature sulfurization treatment. Typically, the FeNiCoS was loaded in a ceramic boat, and 1.0 g of sulfur powders was placed 2 cm away from the foam at the upstream side. Subsequently, the furnace was purged with high-purity Ar (99.9995%) for 1.0 h to get rid of air, heated to 550 °C at a ramping rate of 5 °C min^{-1}, and held at the temperature for 1.5 h.

R-FeNiCoS is synthesized by subjecting the precursor FeNiCoS to a constant current density of 500 mA cm^{-2} for 50 hours in 0.5 M H_2SO_4 electrolyte or acidic seawater.

At last, R-FeNiCoS is synthesized by electrochemical reconstruction after 0, 10 and 50 hours chronoamperometry measurements at a certain potential, labeled as FeNiCoS, R_{10}-FeNiCoS, and R-FeNiCoS, respectively.

1.3 Characterizations

The crystal phases were recorded using the X-ray diffraction by an X-ray powder diffractometer (Bruker D8 advance, Shimadzu Kyoto, Germany) with Cu Kα radiation. The morphologies and composition of the samples were obtained using a field emission scanning electron microscopy (FESEM, Czech TESCAN MIRA LMS, China) and X-ray energy-dispersive spectroscopy (EDS) at an accelerating voltage of 20 kV. The phase structure transmission electron microscopy (TEM, JEOL JEM 2010F, Japan) was examined at 200 kV. The X-ray photoelectron spectroscopy (XPS, K-Alpha, USA) was used to detect the surface elemental composition. The Raman spectra was characterized using a confocal Raman microscope (LabRam HR800, Horiba Jobin Yvon, France) with a laser (532 nm) as the excitation source. Ultraviolet photoelectron spectroscopy (UPS) was performed on Thermo ESCALAB Xi+ equipped with ultraviolet photoelectron spectroscopy (Hel (21.22 eV)). Ex situ and operando Ni K-edge X-ray absorption near-edge structure (XANES) and extended X-ray absorption fine structure (EXAFS) experiments were carried out at the European Synchrotron Radiation Facility (ESRF), Swiss-Norwegian Beamline BM31, Grenoble, France. Athena and Artemis were used for processing the XAS data.

1.4 Electrochemical measurements

The hydrogen evolution reaction (HER) activities were conducted at room temperature using a workstation (CS300, Wuhan Corrtest Instrument Corp., Ltd) in 0.5 M H_2SO_4+0.5 M NaCl. A standard three-electrode system was used, in which the synthesized catalysts as the working electrode, carbon rod served as the counter electrode, and a standard $Hg/HgSO_4$ electrode filled with 0.5 M H_2SO_4 solution as the reference electrode. The effective area of the working electrode is 1.0 cm × 1.0 cm. The linear sweep voltammetry (LSV) was evaluated at a scan rate of 5 mV s^{-1}, which was adjusted with 90% iR correction to minimize the influence of ohmic resistance. Electrochemical impedance spectroscopy (EIS) was carried out in the same configuration at an overpotential of 200 mV from 0.1 Hz to 100 kHz with an amplitude of 10 mV. All potentials in the work were converted to a reversible hydrogen electrode by adding -0.21473 V based on the Nernst equation ($E_{RHE}=E_{Hg/HgSO4}+0.059\times pH+0.14$). The overpotential (η) of HER was calculated according to the following formula: η (V) $=E_{RHE}$ - 0 V. Measurements of electrochemical active surface area (ECSA) were estimated following equation: $ECSA = C_{dl}/C_s$, where the value of C_s is about 40 μF cm^{-2}. The double-layer capacitance (C_{dl}) from the CV curves at the five scan rates (60, 70, 80, 90, and 100 mV s^{-1}) in the potential range from 0.72 V ~ 0.82 V (*vs.*RHE), which is equivalent to the slopes of linear plots from the current density at 0.90 V. The stability of the electrode was measured by applying a constant potential to achieve a current density of 100 mA cm^{-2} for 100 hours. The oxygen generated from a couple of two-electrode systems at 100 mA cm^{-2} was collected via the drainage method.

1.5 PEM Measurement.

To prepare the membrane electrode assembly (MEA), the Nafion 117 membrane (N117, Dupont) was sequentially treated with 3 wt% H_2O_2, 0.5 M H_2SO_4, and distilled water at 80 °C for 1 hour each. After cooling to room temperature, the treated N117 membrane was stored in distilled water. For the PEM cell, R-FeNiCoS catalyst or commercial Pt/C (40 *wt*%) was used as the cathode catalyst, and commercial IrO_2 was used as the anode catalyst.

The PEM electrolytic cell was operated at both room temperature and 80 °C, using 0.5 M H_2SO_4 electrolyte solution circulated at a flow rate of 20 mL min^{-1} via a peristaltic pump. The performance of the PEM electrolysis cell was evaluated by measuring the polarization curve (LSV) from 0 to 2 A cm^{-2} using an electrochemical workstation. The stability was assessed by applying a constant potential current method at 500 mA cm^{-2} for 100 hours.

1.6 DFT Calculations

Density Functional Theory (DFT) simulations were studied by employing Cambridge Sequential Total Energy Package (CASTEP) module implemented in Material Studio. In CASTEP module, to account for exchange-correlation effects, the generalized gradient approximation (GGA) with the Perdew-Burke-Ernzerh of (PBE) exchange-correlation functional model was used in the calculations. The cut off energy of the plane wave basis set is 550 eV, and a Monkhorst mesh of 2×2×4 was considered in K-sampling. All calculations for the slab model were evaluated on a 1× 1×1 Gamma-centered Monkhorst-Pack k-point grid. For the geometric structure optimization, the criterions until energy change, max force on each atom, stress and max displacement are less than 10^{-5} eV/atom, 0.03 eV/Å, 0.05 GPa and 10^{-3} Å, respectively. The spin-polarized calculations were

performed to relax the structures until the force and energy on each atom is smaller than 1.0×10^{-5} eV/Å. In our calculations, the hydrygen intermediates were adsorbed on the R-FeNiCoS (020) surface following a previous method.

2. Supplementary Figures

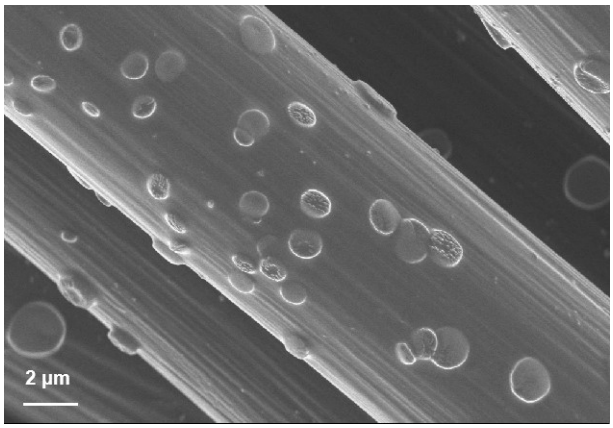

Supplementary Fig.S1. The resolution SEM images of R-FeNiCoS.

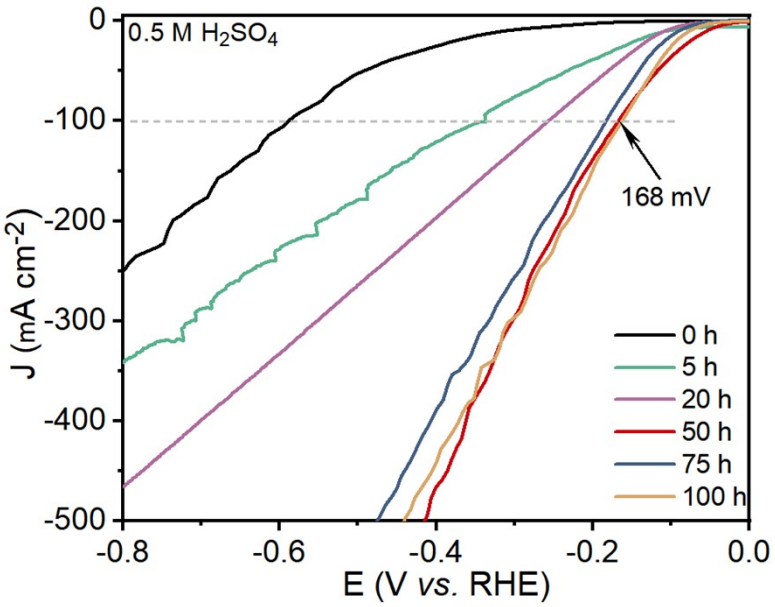

Supplementary Fig.S2 The images of systematically characterize the R-FeNiCoS as a function of reconstruction time and applied potential.

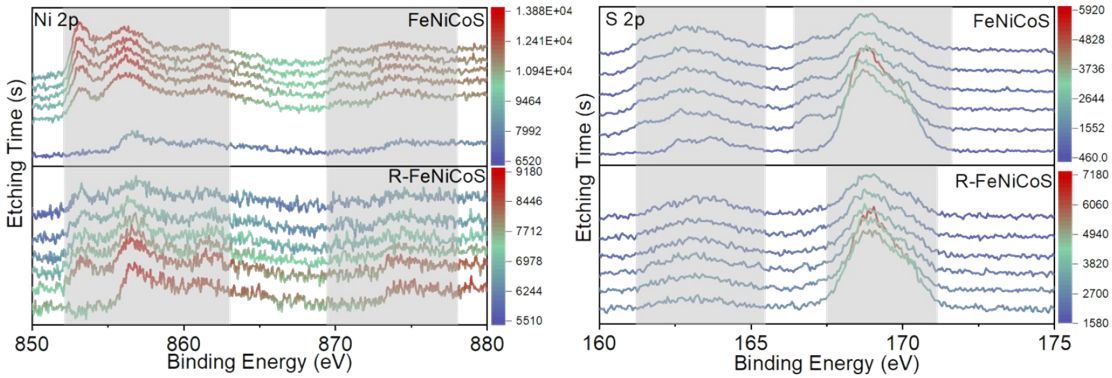

Supplementary Fig.S3 XPS survey spectrum of **(a)** Ni 2p and **(b)** S 2p regions of R-FeNiCoS.

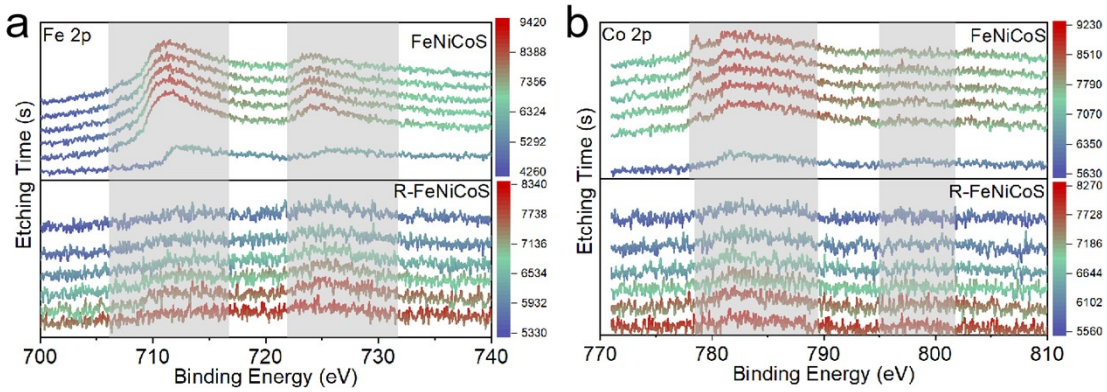

Supplementary Fig.S4 XPS survey spectrum of **(a)** Fe 2p and **(b)** Co 2p regions of R-FeNiCoS.

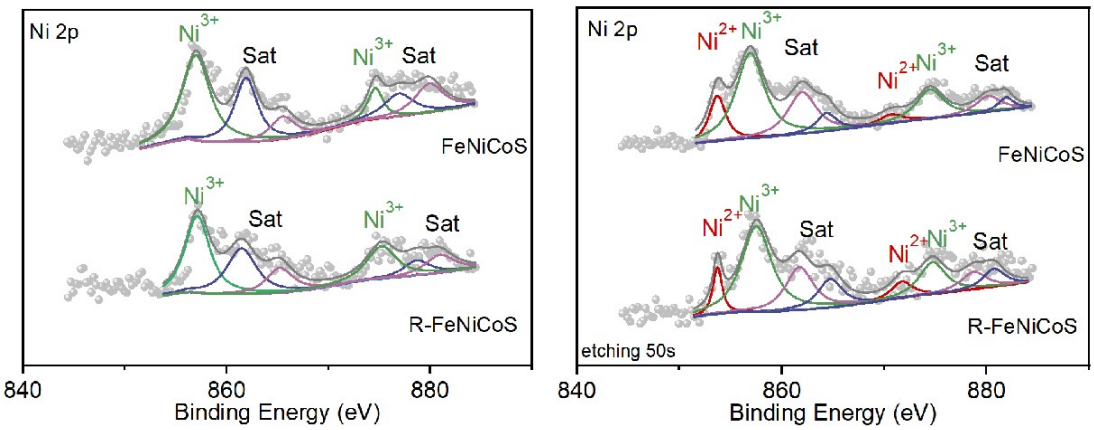

Supplementary Fig.S5 XPS survey spectrum of Ni 2p regions **(a)** in etching 0s and **(b)** in etching 50s of R-FeNiCoS and FeNiCoS.

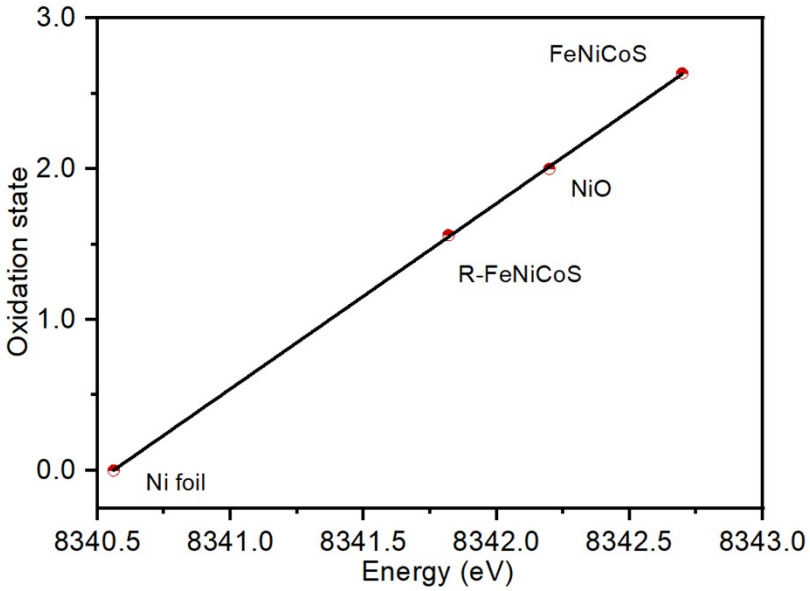

Supplementary Fig.S6 The Ni valence states of R-FeNiCoS and FeNiCoS fitted by Ni K-edge absorption energy at different potentials.

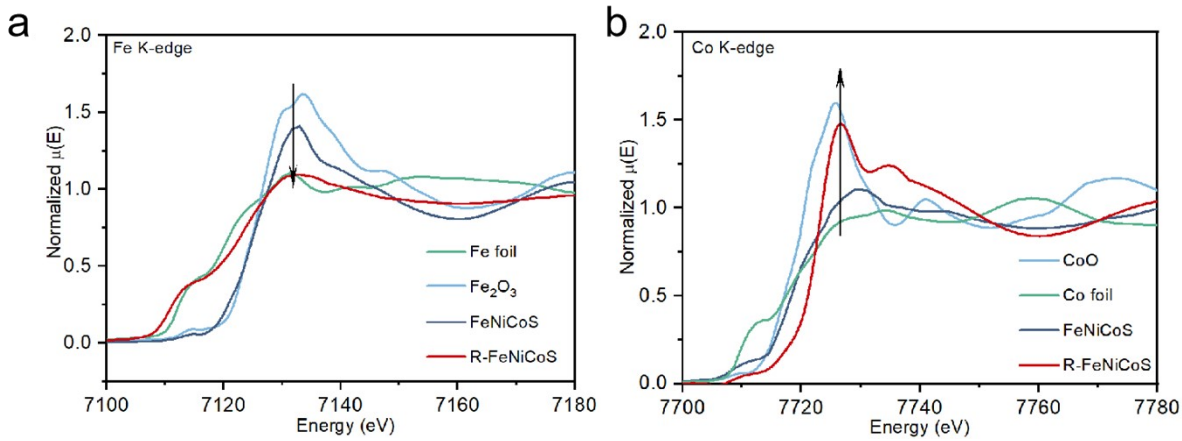

Supplementary Fig.S7 XANES spectra of (a) Fe K-edge and (b) Co K-edge.

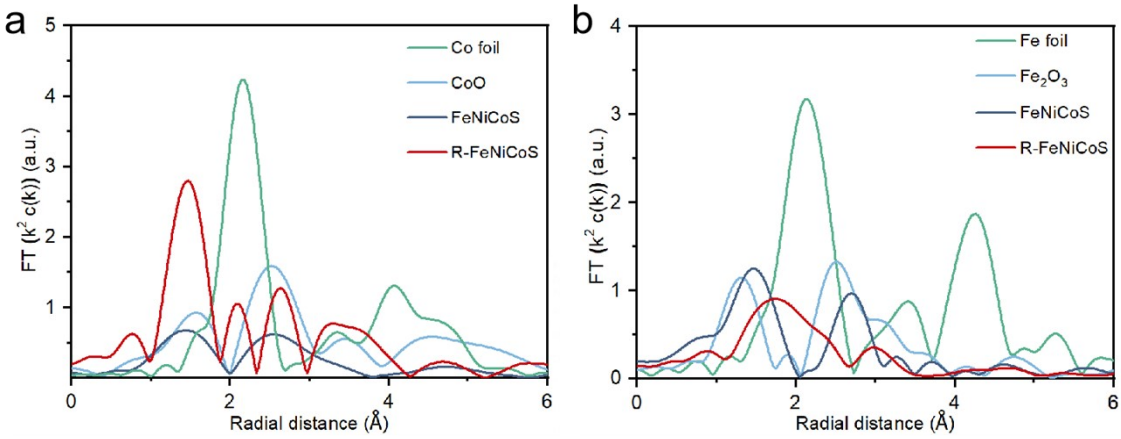

Supplementary Fig.S8 FT-EXAFS spectra of (a) Fe K-edge and (b) Co K-edge.

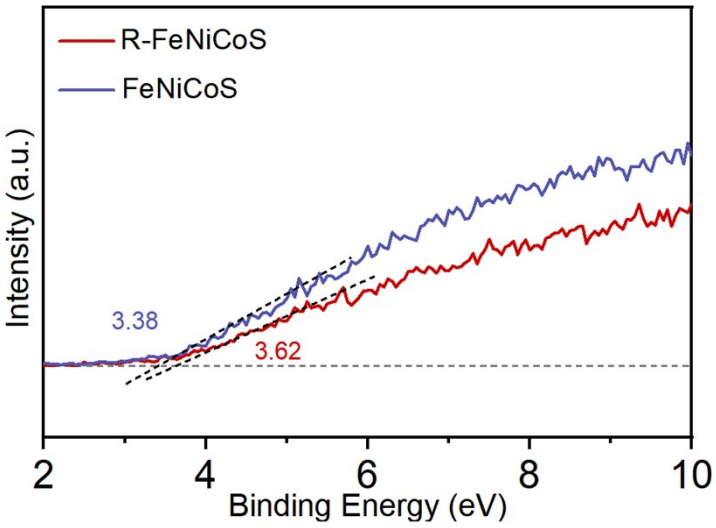

Supplementary Fig.S9 Valence-band spectrum.

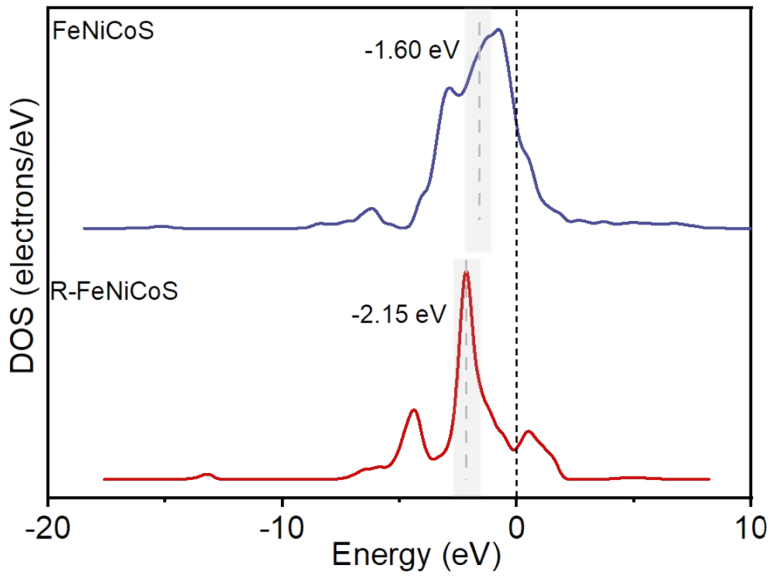

Supplementary Fig.S10 The calculated d-band center of R-FeNiCoS.

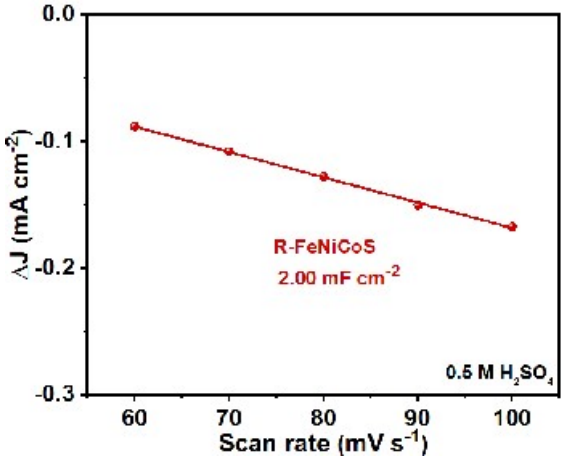

Supplementary Fig.S11 The CV curves of (a) R-FeNiCoS, (b) carbon cloth in the non-Faraday reaction region at different scan rates of 10, 20, 30, 40, 50 and 60 mV s^{-1} in 0.5 M H_2SO_4.

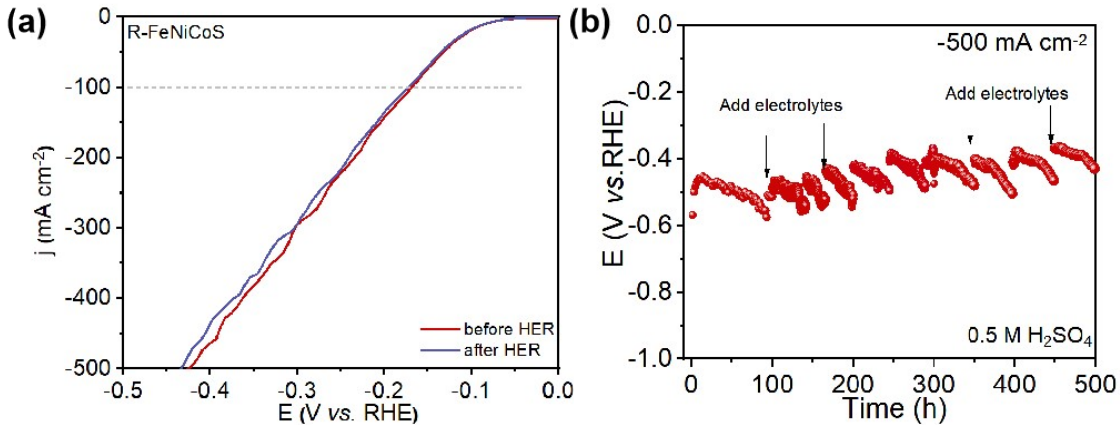

Supplementary Fig.S12 (a) Polarization curves of R-FeNiCoS before (red) and after (blue) long-time stability. **(b)** R-FeNiCoS at constant current densities for HER in 0.5 M H_2SO_4 electrolyteR-FeNiCoS at constant current densities of 500 mA cm^{-2} for 500 hours for HER in 0.5 M H_2SO_4 electrolyte.

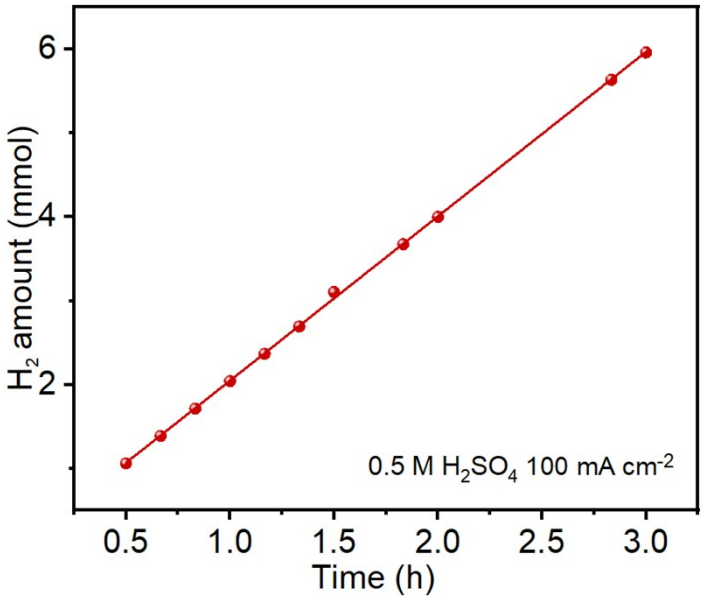

Supplementary Fig.S13 Generated H_2 amounts for the assembled electrolyzer.

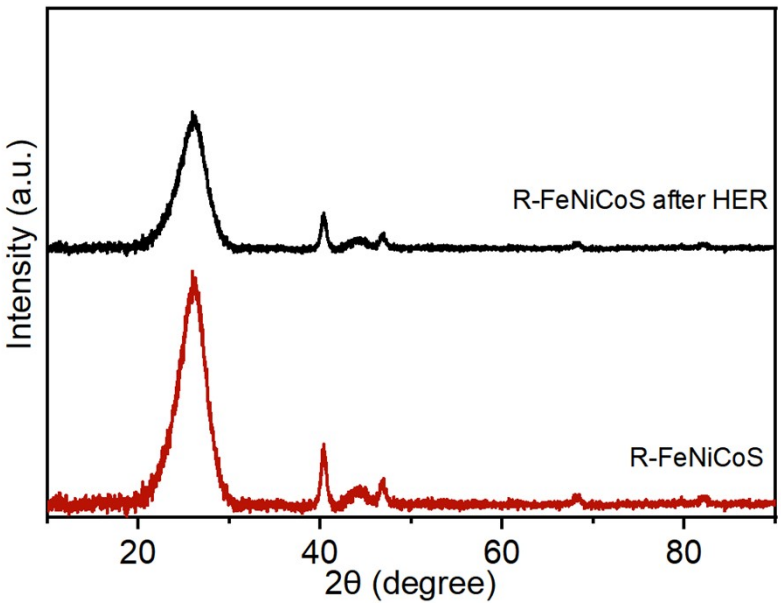

Supplementary Fig.S14 XRD patterns of the R-FeNiCoS before and after HER.

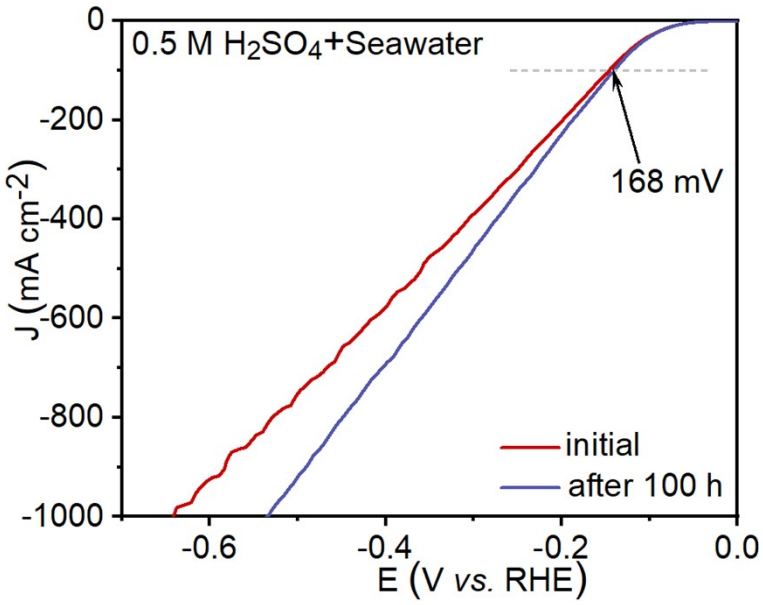

Supplementary Fig.S15 LSV curves of R-FeNiCoS for HER in 0.5 M H_2SO_4 + seawater.

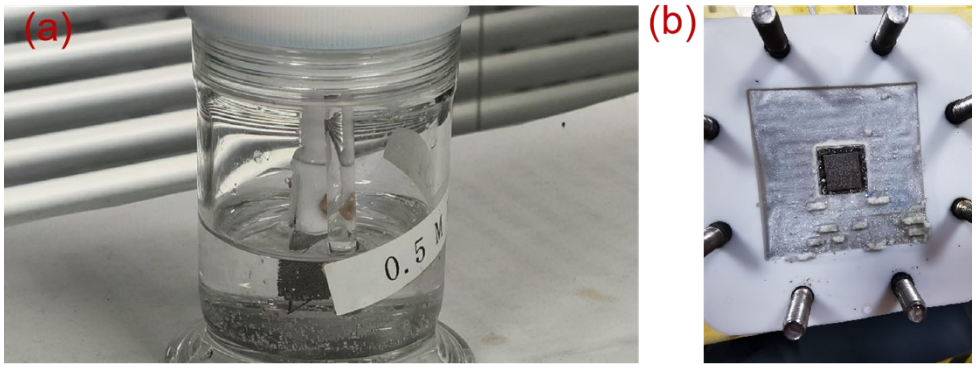

Supplementary Fig.S16 (a) Photograph of the R-FeNiCoS cathode. (b) Photograph of the R-FeNiCoS cathode for HER in PEMWE device, using 0.5 M H_2SO_4 in seawater as the electrolyte.

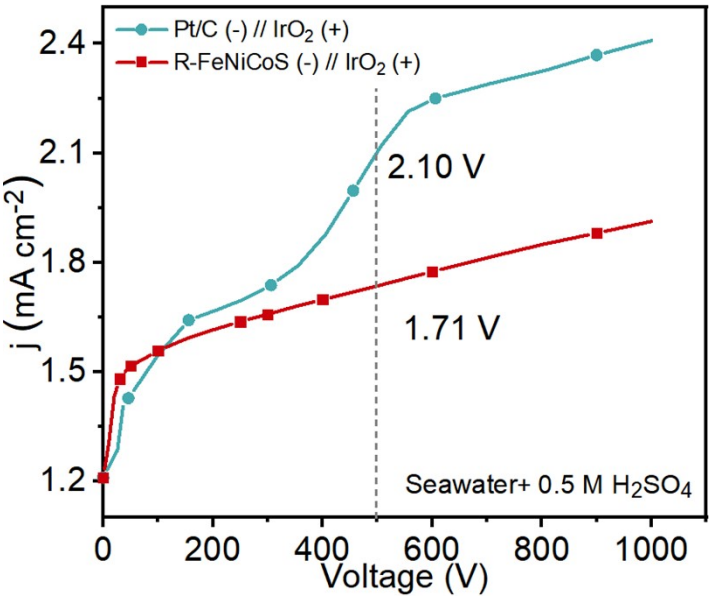

Supplementary Fig.S17 Polarization curves of the PEM electrolyser using 0.5 M H_2SO_4 in seawater as the electrolyte operated at 80 °C.

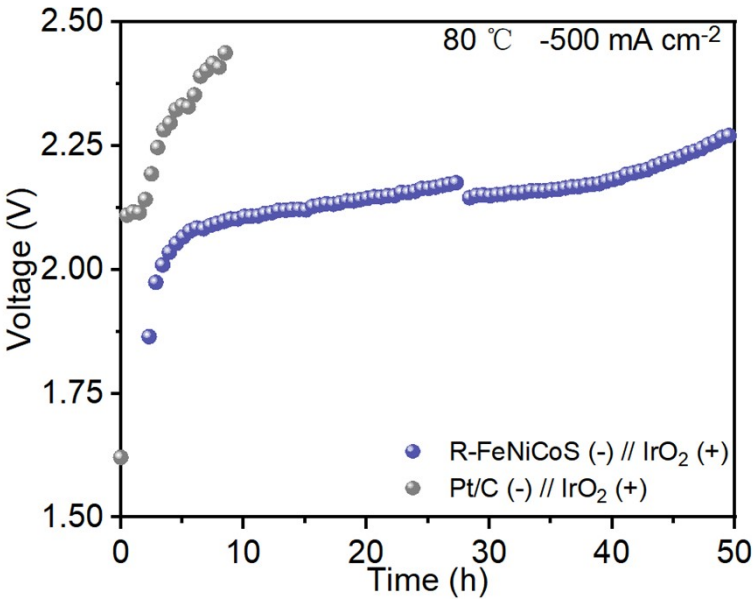

Supplementary Fig.S18 Durability test of the PEMWE electrolyser using 0.5 M H_2SO_4 in seawater as the electrolyte operated at 80 °C.

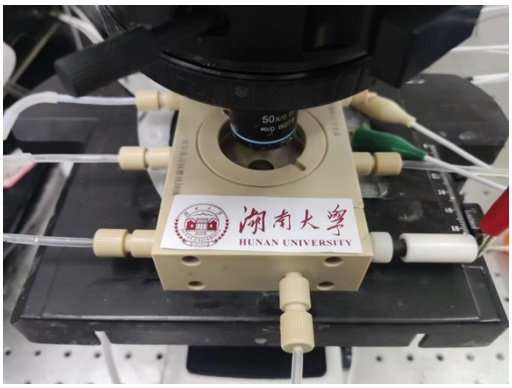

Supplementary Fig.S20 Electrochemical cell for operando Raman measurements. The experimental set-up for operando Raman measurement. W.E., R.E. and C.E. stand for working electrode (R-FeNiCoS catalyst), reference electrode (Ag/AgCl) and counter electrode (carbon rods), respectively.

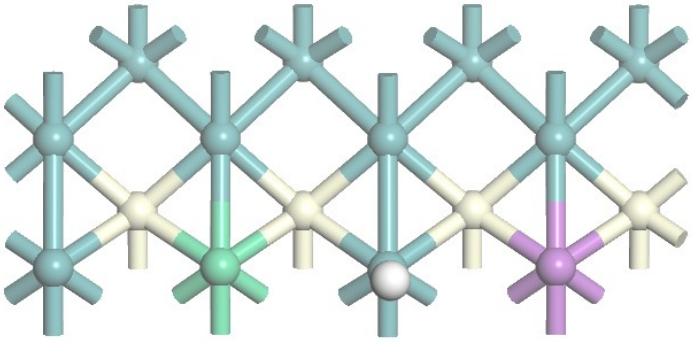

Supplementary Fig.S21 The optimized structures of H* adsorbed on Ni site for R-FeNiCoS.

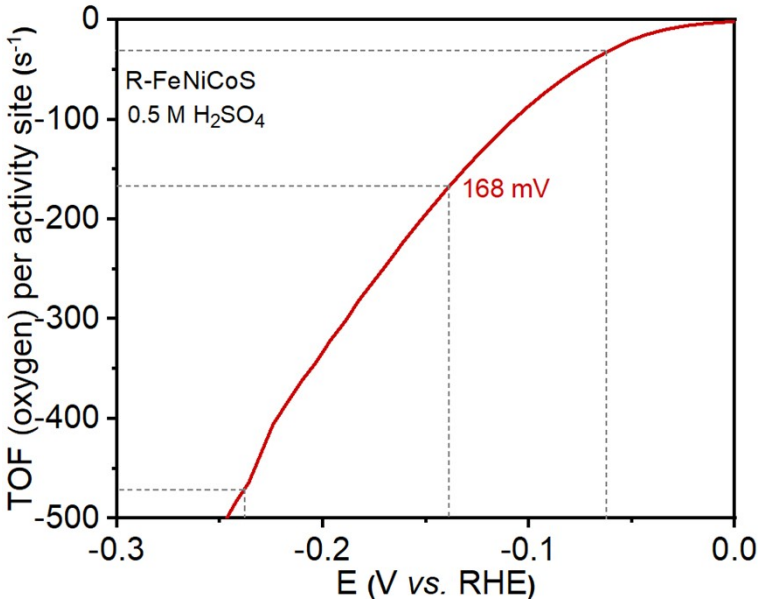

Supplementary Fig.S22 TOF curves of the corresponding of R-FeNiCoS electrodes for HER.

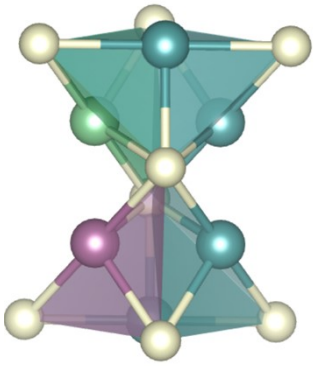

Volume: 206.076 Å

Contains: 4 Ni, Co, Fe, 8 S

In which Ni:blue atoms, Co: purple atoms, Fe: green atoms, S: orange atoms

Calculation details of ECSA:

ECSA = C_{dl}/C_s, C_s=40 μF cm^{-2}

$ECSA_{R\text{-}FeNiCoS/CC}$ = 2.00 mF cm^{-2}/40 μF cm^{-2}= 50 cm^{-2} $_{ECSA}$

The Turnover Frequency (TOF) Calculation is defined as the rate of evolved molecular H_2 per surface active site per second, which can be calculated by the following equation:

$$\mathrm{TOF}(s^{-1}) = \frac{\text{number of hydrogen turnovers / cm}^2 \text{ of geometric area}}{\text{number of active sites/cm}^2 \text{ of geometric area}}$$ Eq. (A.1)

The number of TOF for HER was calculated from the current density according to:

$$\text{number of hydrogen turnover} = (\mathrm{j}\frac{\mathrm{mA}}{\mathrm{cm}^2})(\frac{1C/s}{1000mA})(\frac{1mole^-}{96485.3C})(\frac{1molH_2}{2mole^-}) \times 6.023\times10^{23}$$ Eq. (A.2)

At an overpotential of 62, 168, and 238 mV the R-FeNiCoS reached a current density of 10, 100, and 500 mA cm^{-2}, respectively.

Number of hydrogen turnover for R-FeNiCoS at 62 mV overpotential

$$\text{number of hydrogen turnover} = (10\frac{\mathrm{mA}}{\mathrm{cm}^2})(\frac{1C/s}{1000mA})(\frac{1mole^-}{96485.3C})(\frac{1molH_2}{2mole^-}) \times 6.023\times10^{23} = 3.12\times10^{16}(\frac{1/s}{cm^2})$$

number of hydrogen turnover for R-FeNiCoS at 168 mV overpotential

$$\text{number of hydrogen turnover} = (100\frac{\mathrm{mA}}{\mathrm{cm}^2})(\frac{1C/s}{1000mA})(\frac{1mole^-}{96485.3C})(\frac{1molH_2}{2mole^-}) \times 6.023\times10^{23} = 3.12\times10^{17}(\frac{1/s}{cm^2})$$

number of hydrogen turnover for R-FeNiCoS at 238 mV overpotential

$$\text{number of hydrogen turnover} = (500\frac{\mathrm{mA}}{\mathrm{cm}^2})(\frac{1C/s}{1000mA})(\frac{1mole^-}{96485.3C})(\frac{1molH_2}{2mole^-}) \times 6.023\times10^{23} = 1.56\times10^{18}(\frac{1/s}{cm^2})$$

The nature of the active sites is not yet understood, we thus estimated all surface atoms as active sites based on Wu's work [1], which may underestimate the real TOF. The active sites can be calculated using following equations and corresponding the unit cell (volume of 89.9613 Å^3) of R-FeNiCoS crystal structure (Ni, Fe, Co and S is considered as the active site) shown in Figure S8:

$$Active\ sites = (\frac{4\ atom/unit\ cell}{89.9613/unit\ cell})^{2/3} = 0.13\times10^{14}\ atom\ cm^2{}_{real}$$ Eq. (A.3)

$$TOF(n_{62}) = \frac{3.12\times10^{16}\ \frac{\mathrm{mA}}{\mathrm{cm}^2}}{sueface\ sites\times ECAS} = \frac{3.12\times10^{16}\ \frac{\mathrm{mA}}{\mathrm{cm}^2}}{0.13\times10^{14}\times50} = 0.48\times10^{2}\ \mathrm{s}^{-1}$$

$$TOF(n_{168}) = \frac{3.12\times10^{17}\ \frac{\mathrm{mA}}{\mathrm{cm}^2}}{sueface\ sites\times ECAS} = \frac{3.12\times10^{17}\ \frac{\mathrm{mA}}{\mathrm{cm}^2}}{0.13\times10^{14}\times50} = 0.48\times10^{3}\ \mathrm{s}^{-1}$$

$$TOF(n_{238}) = \frac{1.56\times10^{18}\ \frac{\mathrm{mA}}{\mathrm{cm}^2}}{sueface\ sites\times ECAS} = \frac{1.56\times10^{18}\ \frac{\mathrm{mA}}{\mathrm{cm}^2}}{0.13\times10^{14}\times50} = 0.24\times10^{4}\ \mathrm{s}^{-1}$$

Supplementary Table S1. XPS of R-FeNiCoS

Elements	Atomic %
Fe	3.66
Ni	9.20
Co	1.88
S	85.26

Supplementary Table S2. Thermodynamic data used in the free energy analysis

Active Sites	E	ZPE	-TS	ΔG
Ni site	-1.6509	0.186398	-0.00393658	-1.4685
Co site	-1.6821	0.171069	-0.01103494	-1.5221
Fe site	-1.6717	0.149058	-0.00105194	-1.5237
S site	-1.6412	0.160484	-0.02405754	-1.5048

Supplementary Table S3. Summary of some recently reported representative HER non-precious electrocatalysts in acidic medium (0.5 M H_2SO_4).

Catalyst	Media	$\eta_{j=}$10 mA cm^{-2}	Tafel slope (mV dec^{-1})	Ref
R-FeNiCoS	0.5 M H_2SO_4	62	**71**	**this work**
Ni/Fe_3C	0.5 M H_2SO_4	112	206	[1]
Ni/VC	0.5 M H_2SO_4	111	86	
$CoSe_2$/CoP	0.5 M H_2SO_4	65	54	[2]
MoO_2/MoS_2/C	0.5 M H_2SO_4	77	41	[3]
MoP/Mo_2N	0.5 M H_2SO_4	91	78	[4]
W_2S_3	0.5 M H_2SO_4	75	36	[5]
Mo_2CT_x:Co	0.5 M H_2SO_4	180	59	[6]
P-MoP/Mo_2N	0.5 M H_2SO_4	89	53	[7]
MoS_xCl	0.5 M H_2SO_4	150	48	[8]
$WS_{1.14}Se_{0.86}$	0.5 M H_2SO_4	80	85	[9]
MoS_2/$CoSe_2$	0.5 M H_2SO_4	75	36	[10]
M-$CoSe_{1.28}S_{0.72}$	0.5 M H_2SO_4	67	50	[11]
Ni-doped FeP/C	0.5 M H_2SO_4	72	54	[12]
NiCu	0.5 M H_2SO_4	81	87.4	[13]

Supplementary Table S4. Comparison of the performance of PEMWE with the non-noble metal cathodes.

Catalyst	Current (mA cm^{-2})	Cell Temp (℃)	Cell voltage (V)	
R-FeNiCoS‖IrO_2	1000	80	1.81	**this work**
W_2S_3‖IrO_2	1000	60	1.73	[5]
M-$CoSe_{1.28}S_{0.72}$ ‖IrO_2	1000	60	1.79	[11]
CoP‖IrO_2	1000	50	2.05	[14]

Supplementary Table S5. Comparison of the performance of PEMWE with the non-noble metal anodes.

Catalyst	Current (mA cm^{-2})	Cell Temp (℃)	Cell voltage (V)	
W–Co_3O_4‖Pt/C	500	50	1.72	[15]
	1000		1.83	
CoFeNiMoWTe‖Pt/C	10	70	1.63	[16]
LD-B/RuO_2‖ Pt/C	500	80	1.53	[17]
	1000		1.63	
γ-MnO_2‖ Pt/C	1000	80	2.00	[18]

Supplementary Table S6. Summary of seawater splitting using transition-metal catalysts.

Electrocatalyst	Electrolyte	Overpotential (mV)	Ref.
Ni_2P-Fe_2P/NF	1.0 M KOH	261 （at 100 mA/cm^2)	[19]
		337（at 1000 mA/cm^2)	
	1.0 M KOH+seawater	305（at 100 mA/cm^2)	
		431（at 1000 mA/cm^2)	
NiFe/NiS-Ni	1.0 M KOH	1.72V （at 400 mA/cm^2)	[20]
	6.0 M KOH+1.5 M NaCl	2.1V（at 400 mA/cm^2)	
NiMoN/NiMoN	1.0 M KOH	277 （at 100 mA/cm^2) 337（at 500 mA/cm^2)	[21]
	1.0 M KOH+0.5 M NaCl	286（at 100 mA/cm^2) 347（at 500 mA/cm^2)	
	1.0 M KOH+Seawater	307（at 100 mA/cm^2) 369（at 500 mA/cm^2) 398（at 1000mA/cm^2)	
NiCoFeP	6.0 M KOH+2.8 M NaCl	272（at 100 mA/cm^2)	[22]

h-$Co_{0.34}Fe_{0.33}Ni_{0.33}$-LDH	1.0 M KOH	195（at 10 mA/cm^2)	[23]
CoP/CoMoP	0.5 M H_2SO_4	$\eta_{10mA/cm2}$=72mV	[24]
FeP-Ni/NF	1.0 M KOH	218（at 10 mA/cm^2)	[25]
H-FeNiP	1.0 M KOH	252（at 10 mA/cm^2)	[26]
NPNNS	1.0 M KOH	87（at 10 mA/cm^2)	[27]
	Neutral seawater media	144（at 10 mA/cm^2)	
	0.5 M H_2SO_4	66（at 10 mA/cm^2)	
$CrMnFeCoNiS_x$		$\eta_{100mA/cm}{}^2$=295mV	[28]
$Ni_{0.8}Fe_{0.2}$-AHNA	1.0 M KOH	190（at 100 mA/cm^2) 248（at 500 mA/cm^2) 258（at 1000mA/cm^2)	[29]
$Zn_{0.4}Ni_{0.6}Co_2O_4$/NCNTs	0.1 M KOH	$E_{10mA/cm}{}^2$=1.64 mV	[30]
$Mn_{0.52}Fe_{0.71}$Ni-MOF-74	1.0 M KOH	$\eta_{100mA/cm}{}^2$=267mV	[31]

$(Ni_{0.66}Fe_{0.33})_2P$	1.0 M KOH	η_{10mA/cm^2}=182mV η_{50mA/cm^2}=280mV η_{100mA/cm^2}=325mV	32
NiFe-LDH	1.0 M KOH	η_{10mA/cm^2}=324mV η_{100mA/cm^2}=430mV	33
Ni-doped FeOOH	1.0 M KOH+Seawater	η_{100mA/cm^2}=301 mV	
0.5Fe-$NiCo_2O_4$@CC	1.0 M KOH	$\eta_{10\ mA/cm^2}$ =258 mV	34
	1.0 M KOH+0.5 M NaCl	$\eta_{10\ mA/cm^2}$ =273 mV	
	1.0 M KOH+Seawater	$\eta_{10\ mA/cm^2}$ =293 mV	
S-(Ni,Fe)OOH	1.0 M KOH	$\eta_{100\ mA/cm^2}$ =229 mV, $\eta_{500\ mA/cm^2}$ =281 mV， $\eta_{500\ mA/cm^2}$ =328 mV $\eta_{1000\ mA/cm^2}$ =355 mV	35
	1.0 M KOH+0.5 M NaCl	$\eta_{100\ mA/cm^2}$ =278 mV, $\eta_{500\ mA/cm^2}$ =339mV $\eta_{1000\ mA/cm^2}$ =378 mV	
	1.0 M KOH+Seawater	$\eta_{100\ mA/cm^2}$ =300 mV $\eta_{500\ mA/cm^2}$ =398 mV $\eta_{1000\ mA/cm^2}$ =492 mV	
MoO*x*@NCHSs-750	1.0 M KOH	$\eta_{10\ mA/cm^2}$ =160 mV	

MoO*x*@NCHSs-800		$\eta_{10\ mA/cm^2}$ =144mV	
MoO*x*@NCHSs-900		$\eta_{10\ mA/cm^2}$ =92 mV	
$Ni_3Bi_2S_2$	1.0 M KOH	$\eta_{10\ mA/cm^2}$ =127 mV	36
	1.0 M KOH+0.5 M NaCl	$\eta_{100\ mA/cm^2}$ =390 mV	
NiFe-MOF/NF	1.0 M KOH	$\eta_{10\ mA/cm^2}$=206 mV, $\eta_{100\ mA/cm^2}$=232.7 mV	37
N-WS_2/Ni_3FeN	1.0 M KOH	$\eta_{100\ mA/cm^2}$=240 m V $\eta_{500\ mA/cm^2}$=285 mV	38
CoZn MOF/CC	1.0 M KOH	$\eta_{10\ mA/cm^2}$ = 287	39
$NiFeO_x$	1.0 M KOH	$\eta_{20\ mA/cm^2}$=230 mV	40
Pt/Ni-MOF-C	1.0 M KOH	$\eta_{10\ mA/cm^2}$=66 mV	41
	0.5 M H_2SO_4	$\eta_{100\ mA/cm^2}$=28 mV	
FeP/Ni_2P	1.0 M KOH	$\eta_{10\ mA/cm^2}$=154 mV	42
$Co(OH)_2$-ZIF-L/NF-40	0.1 M KOH	$\eta_{100\ mA/cm^2}$=290mV, $\eta_{500\ mA/cm^2}$=359 mV	43
$NiFeO_xH_y$-PN	1.0 M KOH	$\eta_{100\ mA/cm^2}$=265 mV $\eta_{1000\ mA/cm^2}$=326 mV	44

Ni-W-B (without PTE)	1.0 M KOH	$\eta_{10\ mA/cm^2}$=211 mV $\eta_{100\ mA/cm^2}$=367 mV	45
Ni-W-B (PTE)		$\eta_{50\ mA/cm^2}$=191 mV $\eta_{100\ mA/cm^2}$=344 mV	
CC-NC-NiFeP	1.0 M KOH	$\eta_{10\ mA/cm^2}$=145 mV	46
Fe - CoP HTPAs	1.0 M KOH	$\eta_{10\ mA/cm^2}$=230 mV	47
EP NiFe LDH/Ni-Cotton	1.0 M KOH	$\eta_{50\ mA/cm^2}$=214mV $\eta_{100\ mA/cm^2}$=228 mV	48
γ-FeOOH/NF	1.0 M KOH	$\eta_{10\ mA/cm^2}$=286±3 mV $\eta_{100\ mA/cm^2}$=316±3 mV	49
（N，S）-RGO/CoN	PH=7	$\eta_{10\ mA/cm^2}$=220 mV	50
MoO_3@CoO/CC	1.0 M KOH+0.5 M NaCl	$\eta_{100\ mA/cm^2}$=389 mV	51
NiMoN@N-iFeN	1.0 M KOH+0.5 M NaCl	$\eta_{100\ mA/cm^2}$=307 mV	21
CoFe-Ci@GQDs/NF	1.0 M KOH+0.5 M NaCl	$\eta_{100\ mA/cm^2}$=255 mV	52

References

1. C. Yang, R. Zhao, H. Xiang, J. Wu, W. Zhong, W. Li, Q. Zhang, N. Yang and X. Li, *Advanced Energy Materials*, 2020, **10**.
2. S. Shen, Z. Wang, Z. Lin, K. Song, Q. Zhang, F. Meng, L. Gu and W. Zhong, *Advanced Materials*, 2022, **34**.
3. F. Gong, M. Liu, S. Ye, L. Gong, G. Zeng, L. Xu, X. Zhang, Y. Zhang, L. Zhou, S. Fang and J. Liu, *Advanced Functional Materials*, 2021, **31**, 2101715.
4. Y. Gu, A. Wu, Y. Jiao, H. Zheng, X. Wang, Y. Xie, L. Wang, C. Tian and H. Fu, *Angewandte Chemie International Edition*, 2021, **60**, 6673-6681.
5. L. Xie, L. Wang, X. Liu, W. Zhao, S. Liu, X. Huang and Q. Zhao, *Angewandte Chemie International Edition*, 2023, **63**.
6. D. A. Kuznetsov, Z. Chen, P. V. Kumar, A. Tsoukalou, A. Kierzkowska, P. M. Abdala, O. V. Safonova, A. Fedorov and C. R. Müller, *Journal of the American Chemical Society*, 2019, **141**, 17809-17816.
7. H. Fu, Y. Gu, A. Wu, Y. Jiao, H. Zheng, X. Wang, Y. Xie, L. Wang and C. Tian, *Angewandte Chemie International Edition*, 2020, DOI: 10.1002/anie.202016102.
8. Q. Ding, J. Zhai, M. Cabán-Acevedo, M. J. Shearer, L. Li, H. C. Chang, M. L. Tsai, D. Ma, X. Zhang, R. J. Hamers, J. H. He and S. Jin, *Advanced Materials*, 2015, **27**, 6511-6518.
9. Q. Fu, L. Yang, W. Wang, A. Han, J. Huang, P. Du, Z. Fan, J. Zhang and B. Xiang, *Advanced Materials*, 2015, **27**, 4732-4738.
10. M.-R. Gao, J.-X. Liang, Y.-R. Zheng, Y.-F. Xu, J. Jiang, Q. Gao, J. Li and S.-H. Yu, *Nature Communications*, 2015, **6**.
11. P. Y. XiaoLong Zhang, XiaoZhi Su, ShaoJin Hu, Lei Shi, YeHua Wang, PengPeng Yang, FeiYue Gao, Zhi-Zheng Wu, Li-Ping Chi, Ya-Rong Zheng, Min-Rui Gao, *Science Advances*, 2024, **9**.
12. L. Y. Xue Feng Lu, Xiong Wen Lou *Science Advances*, 2019.
13. Y. Shen, Y. Zhou, D. Wang, X. Wu, J. Li and J. Xi, *Advanced Energy Materials*, 2017, **8**.
14. L. A. King, M. A. Hubert, C. Capuano, J. Manco, N. Danilovic, E. Valle, T. R. Hellstern, K. Ayers and T. F. Jaramillo, *Nature Nanotechnology*, 2019, **14**, 1071-1074.
15. J. Cao, D. Zhang, B. Ren, P. Song and W. Xu, *Energy & Environmental Science*, 2024, **17**, 5911-5921.
16. S. Jo, M. C. Kim, K. B. Lee, H. Choi, L. Zhang and J. I. Sohn, *Advanced Energy Materials*, 2023, **13**, 2301420.
17. G. Chen, R. Lu, C. Ma, X. Zhang, Z. Wang, Y. Xiong and Y. Han, *Angewandte Chemie International Edition*, 2024, DOI: 10.1002/anie.202411603.
18. S. Kong, A. Li, J. Long, K. Adachi, D. Hashizume, Q. Jiang, K. Fushimi, H. Ooka, J. Xiao and R. Nakamura, *Nature Catalysis*, 2024, **7**, 252-261.
19. L. Wu, L. Yu, F. Zhang, B. McElhenny, D. Luo, A. Karim, S. Chen and Z. Ren, *Advanced Functional Materials*, 2020, DOI: 10.1002/adfm.202006484, 2006484.
20. Y. Kuang, M. J. Kenney, Y. Meng, W.-H. Hung, Y. Liu, J. E. Huang, R. Prasanna, P. Li, Y. Li, L. Wang, M.-C. Lin, M. D. McGehee, X. Sun and H. Dai, *Proceedings of the National Academy of Sciences*, 2019, **116**, 6624-6629.
21. L. Yu, Q. Zhu, S. Song, B. McElhenny, D. Wang, C. Wu, Z. Qin, J. Bao, Y. Yu, S. Chen and

Z. Ren, *Nature Communications*, 2019, **10**.

22. P. Li, S. Wang, I. A. Samo, X. Zhang, Z. Wang, C. Wang, Y. Li, Y. Du, Y. Zhong, C. Cheng, W. Xu, X. Liu, Y. Kuang, Z. Lu and X. Sun, *Research*, 2020, **2020**, 1-9.
23. H. Sun, L. Chen, Y. Lian, W. Yang, L. Lin, Y. Chen, J. Xu, D. Wang, X. Yang, M. H. Rümmerli, J. Guo, J. Zhong, Z. Deng, Y. Jiao, Y. Peng and S. Qiao, *Advanced Materials*, 2020, DOI: 10.1002/adma.202006784.
24. X. Huang, X. Xu, X. Luan and D. Cheng, *Nano Energy*, 2020, **68**, 104332.
25. G. Liu, Y. Wu, R. Yao, F. Zhao, Q. Zhao and J. Li, *Green Energy & Environment*, 2020, DOI: 10.1016/j.gee.2020.05.009.
26. R. Zhang, G. Wang, Z. Wei, X. Teng, J. Wang, J. Miao, Y. Wang, F. Yang, X. Zhu, C. Chen, E. Zhou, W. Hu and X. Sun, *Journal of Materials Chemistry A*, 2021, **9**, 1221-1229.
27. M.-Sadeeq (Jie Tang) Baloguna, Anlian Pana,∗, Yexiang Tongc,∗, *Applied Catalysis B: Environmental*, 2019, **251**, 181-194.
28. M. Cui, C. Yang, B. Li, Q. Dong, M. Wu, S. Hwang, H. Xie, X. Wang, G. Wang and L. Hu, *Advanced Energy Materials*, 2020, **11**, 2002887.
29. C. Liang, P. Zou, A. Nairan, Y. Zhang, J. Liu, K. Liu, S. Hu, F. Kang, H. J. Fan and C. Yang, *Energy & Environmental Science*, 2020, **13**, 86-95.
30. X. T. Wang, T. Ouyang, L. Wang, J. H. Zhong and Z. Q. Liu, *Angewandte Chemie International Edition*, 2020, **59**, 6492-6499.
31. W. Zhou, Z. Xue, Q. Liu, Y. Li, J. Hu and G. Li, *ChemSusChem*, 2020, **13**, 5647-5653.
32. S. Li, X. Wang, M. Li, J. Liu, C. Li, H. Wu, D. Guo, F. Ye, S. Wang, L. Cheng and A. Liu, *Electrochimica Acta*, 2019, **319**, 561-568.
33. Z. Wang, S. Wang, L. Ma, Y. Guo, J. Sun, N. Zhang and R. Jiang, *Small*, 2021, **17**, 2006770.
34. Y. W. Jin Yang, Jie Yang, Yajun Pang, Xinqiang Zhu, Yinzhuo Lu, Yitian Wu, Jiajie Wang, Hao Chen, Zongkui Kou, Zhehong Shen, Zhenghui Pan, John Wang, *Small*, 2021, **18**, 2106187.
35. L. W. Luo Yu, Brian McElhenny, Shaowei Song, Dan Luo, Fanghao Zhang, Ying Yu, Shuo Chen, Zhifeng Ren, *Energy & Environmental Science*, 2020, DOI: 10.1039/D0EE00921K 10.1039/x0xx00000x, 3439-3446.
36. D. Yao, W. Hao, S. Weng, M. Hou, W. Cen, G. Li, Z. Chen and Y. Li, *Small*, 2022, DOI: 10.1002/smll.202106868, e2106868.
37. F. L. FeiXiang Ma, Yingxue Diao, BinBin Zhou, Jianghua Wu, Fengwen Kang, Zebiao Li, Xufen Xiao, Peng Wang, Jian Lu, Yang Yang Li, *Nano Research*, 2021, DOI: 10.1007/s12274-021-3885-y.
38. L. Z. Jinsong Zeng, Qian Zhou, Liling Liao, Ying Qi, Haiqing Zhou, Dongyang Li, Fengming Cai, Hui Wang, Dongsheng Tang, Fang Yu, *small*, 2021, **18**, 2104624.
39. Z. Y. Jie Wu, Yuanyuan Zhang, Siqi Niu, Jianying Zhao, Siwei Li,* and Ping Xu*, *Small*, 2021, **2105150**, 1-8.
40. J. Wang, L. Ji, S. Zuo and Z. Chen, *Advanced Energy Materials*, 2017, **7**, 1700107.
41. M. Wang, Y. Xu, C.-K. Peng, S.-Y. Chen, Y.-G. Lin, Z. Hu, L. Sun, S. Ding, C.-W. Pao, Q. Shao and X. Huang, *Journal of the American Chemical Society*, 2021, DOI: 10.1021/jacs.1c06006, 1520-5126.
42. F. Yu, H. Zhou, Y. Huang, J. Sun, F. Qin, J. Bao, W. A. Goddard, S. Chen and Z. Ren, *Nature Communications*, 2018, **9**.

43. J. Ding, T. Fan, K. Shen and Y. Li, *Applied Catalysis B: Environmental*, 2021, **292**, 120174.
44. B. Zhong, P. Kuang, L. Wang and J. Yu, *Applied Catalysis B: Environmental*, 2021, **299**, 120668.
45. W. Hao, R. Wu, H. Yang and Y. Guo, *Journal of Materials Chemistry A*, 2019, **7**, 12440-12445.
46. J. Bian, Z. Song, X. Li, Y. Zhang and C. Cheng, *Nanoscale*, 2020, **12**, 8443-8452.
47. E. Hu, J. Ning, D. Zhao, C. Xu, Y. Lin, Y. Zhong, Z. Zhang, Y. Wang and Y. Hu, *Small*, 2018, **14**, 1704233.
48. Y. Ko, J. Park, J. Mo, S. Lee, Y. Song, Y. Ko, H. Lee, Y. Kim, J. Huh, S. W. Lee and J. Cho, *Advanced Functional Materials*, 2021, DOI: 10.1002/adfm.202102530, 2102530.
49. K. Wang, H. Du, S. He, L. Liu, K. Yang, J. Sun, Y. Liu, Z. Du, L. Xie, W. Ai and W. Huang, *Advanced Materials*, 2021, **33**, 2005587.
50. D. Guo, Z. Zeng, Z. Wan, Y. Li, B. Xi and C. Wang, *Advanced Functional Materials*, 2021, **31**, 2101324.
51. L. Zhou, D. Guo, L. Wu, Z. Guan, C. Zou, H. Jin, G. Fang, X. a. Chen and S. Wang, *Nature Communications*, 2024, **15**.
52. R. Fan, C. Liu, Z. Li, H. Huang, J. Feng, Z. Li and Z. Zou, *Nature Sustainability*, 2024, **7**, 158-167.